



**Enhanced Stability of Silicon for Photoelectrochemical  
 Water Oxidation Through Self-Healing Enabled by an  
 Alkaline Protective Electrolyte**

Journal:	<i>Energy &amp; Environmental Science</i>
Manuscript ID	EE-COM-07-2020-002250.R1
Article Type:	Communication
Date Submitted by the Author:	02-Sep-2020
Complete List of Authors:	<p>Fu, Harold; California Institute of Technology, Chemistry and Chemical Engineering          Moreno-Hernandez, Ivan; California Institute of Technology, Chemistry and Chemical Engineering          Buabthong, Pakpoom; California Institute of Technology, Engineering and Applied Science          Papadantonakis, Kimberly; California Institute of Technology, Chemistry and Chemical Engineering          Brunshwig, Bruce; California Institute of Technology , Beckman Institute Molecular Materials Research Center          Lewis, Nathan S.; California Institute of Technology, Chemistry and Chemical Engineering; California Institute of Technology , Beckman Institute Molecular Materials Research Center</p>

## **Enhanced Stability of Silicon for Photoelectrochemical Water Oxidation Through Self-Healing Enabled by an Alkaline Protective Electrolyte**

Harold J. Fu<sup>1</sup>, Ivan A. Moreno-Hernandez<sup>1</sup>, Pakpoom Buabthong<sup>2</sup>, Kimberly M. Papadantonakis<sup>1</sup>, Bruce S. Brunschwig<sup>3</sup>, Nathan S. Lewis<sup>1,3</sup>

<sup>1</sup>Division of Chemistry and Chemical Engineering, 127-72, California Institute of Technology, Pasadena, CA 91125, USA

<sup>2</sup>Division of Engineering and Applied Sciences, California Institute of Technology, Pasadena, CA 91125

<sup>3</sup>Beckman Institute Molecular Materials Research Center, California Institute of Technology, Pasadena, CA 91125, USA

\*Correspondence to: [nslewis@caltech.edu](mailto:nslewis@caltech.edu)

**Abstract:**

Alkaline electrolytes impede the corrosion of Si photoanodes under positive potentials and/or illumination, due to the formation of a  $\text{SiO}_x$  layer that etches 2-3 orders of magnitude more slowly than Si. Hence during water oxidation under illumination, pinholes in protection layers on Si photoanodes result in the local formation of a protective, stabilizing passive oxide on the Si surface. However, operation under natural diurnal insolation cycles additionally requires protection strategies that minimize the dark corrosive etching rate of Si at pinholes. We show herein that addition of  $[\text{Fe}(\text{CN})_6]^{3-}$  to 1.0 M KOH(aq) results in a self-healing process that extends the lifetime to > 280 h of an  $\text{np}^+$ -Si(100) photoanode patterned with an array of Ni catalyst islands operated under simulated day/night cycles. The self-healing  $[\text{Fe}(\text{CN})_6]^{3-}$  additive caused the exposed Si(100) surface to etch > 180 times slower than the Si etch rate in 1.0 M KOH(aq) alone. No appreciable difference in etch rate or facet preference was observed between Si(100) and Si(111) surfaces in 1.0 M KOH(aq) with  $[\text{Fe}(\text{CN})_6]^{3-}$ , indicating that the surface conformally oxidized before Si dissolved. The presence of  $[\text{Fe}(\text{CN})_6]^{3-}$  minimally impacted the faradaic efficiency or overpotential of  $\text{p}^+$ -Si/Ni electrodes for the oxygen-evolution reaction.

**Broader context:**

Electrochemical generation of fuels from sunlight, water, and  $\text{CO}_2$  would allow the energy from sunlight to be stored for use at any time of day or night. A major focus of the scientific community has been to develop devices that are stable and efficient under solar illumination. Practical implementation of photoelectrochemical cells will also however require stability of these devices under diurnally varying insolation, which exposes the photoelectrodes to open-circuit conditions at low illumination intensities and in the dark. Electrodes can become unstable at low illumination conditions, as exemplified by silicon photoanodes in alkaline electrolytes that corrode at open circuit due to the dissolution of a protective silicon oxide film

that forms anodically under illumination. We demonstrate herein that introducing an oxidizing agent to the electrolyte slows corrosion of silicon by oxidizing the surface in the dark. This self-healing process results in negligible performance losses, and can be complemented by additional protection strategies to construct efficient and stable photoelectrochemical systems that exhibit increased stability in both the light and dark.

### **Introduction**

The solar-driven, photoelectrochemical (PEC) generation of sustainable fuels requires the oxidation of water to  $O_2$  (g) as a half-reaction.<sup>1</sup> Silicon (Si) is a promising semiconductor for PEC water oxidation because the small band gap of Si (1.12 eV) is ideal for tandem devices, and surficial Si oxide passivates electrical defects.<sup>2-7</sup> Operation of PEC devices favors strongly alkaline conditions due to the availability of stable, active, and earth-abundant catalysts for the oxygen-evolution reaction (OER) and hydrogen-evolution reaction (HER) as well as the availability of anion exchange membranes that allow for robust product separation with minimal trans-membrane concentration polarization losses.<sup>8-11</sup> However, Si corrodes in a highly alkaline electrolyte, and requires protection strategies such as metal oxide coatings to stabilize the underlying semiconductor.<sup>12-21</sup> These protection layers allow for an electrical connection between the underlying semiconductor and catalytically active sites while physically blocking the electrolyte from reacting with the semiconductor. For instance,  $Ti^{3+}$  defect sites in amorphous  $TiO_2$  allow for hole conductivity while protecting the underlying substrate from corrosion.<sup>12, 22</sup> Structural defects that allow the electrolyte to reach the semiconductor are expected in protective layers formed on devices at scale, and consequently could result in device failure via local corrosion of the semiconductor.<sup>18</sup> Efforts to decrease the pinhole density in  $TiO_2$  layers by depositing more closely packed films have extended the lifetime of photoanodes, but

undercutting of the protective layer via any remaining pinholes inevitably leads to device failure due to pitting corrosion.<sup>23</sup>

Local formation of Si oxide by anodic oxidation or by illumination of the Si surface can produce Si oxide ( $\text{SiO}_x$ ) that enables partial defect-tolerance of the photoelectrode under operation, by forming a passive film at pinholes in the protective layer.<sup>24</sup> This passivating oxide layer etches orders of magnitude more slowly than Si, and subsequently can extend the overall lifetime ( $> 100$  h) of the electrode.<sup>25, 26</sup> The most stable Si photoanodes in alkaline electrolyte have consequently been obtained under continuous illumination conditions, allowing for the formation and maintenance of protective oxide layers wherever the Si directly contacts the alkaline electrolyte.<sup>27-29</sup> In the dark, the electrode would rest at open circuit in alkaline electrolyte, and consequently no anodic driving force is present to oxidize regions of exposed semiconductor.<sup>26, 30</sup> Hence unless a fully pinhole-free protective layer is present, the Si will subsequently etch rapidly by pitting that will eventually undercut the protective coating.

Modification of the electrolyte composition can have significant ramifications on electrode stability. Saturating a borate buffer electrolyte with  $\text{V}^{5+}$  has been shown to suppress corrosion of  $\text{BiVO}_4$  photoanodes by inhibiting dissolution of  $\text{V}^{5+}$  from the photoelectrode.<sup>31</sup> Herein we report a stabilization strategy for Si photoanodes in alkaline media that is inherently distinct from, but complementary to, use of protective metal oxide coatings. Open-circuit corrosion is suppressed by adding ferricyanide ( $[\text{Fe}(\text{CN})_6]^{3-}$ ) to the electrolyte, which acts as an oxidizing agent and converts the surface Si in situ into a protective, passivating  $\text{SiO}_x$  layer.  $[\text{Fe}(\text{CN})_6]^{3-}$  readily reduces to ferrocyanide ( $[\text{Fe}(\text{CN})_6]^{4-}$ ) in a one-electron transfer reaction, and  $[\text{Fe}(\text{CN})_6]^{3-}$  has been previously shown in the micromachining field to anodically passivate Si in potassium hydroxide (KOH), preventing the formation of etch pits.<sup>32, 33</sup> Introducing  $[\text{Fe}(\text{CN})_6]^{3-}$

to the anolyte component of a membrane-separated PEC cell prevents the  $[\text{Fe}(\text{CN})_6]^{4-}$  from being reduced at the cathode but the  $[\text{Fe}(\text{CN})_6]^{4-}$  is reoxidized under illumination. This strategy allows for anodic passivation to occur through two different pathways for operation both under illumination and in the dark. An advantage of the protective electrolyte protection scheme is that the electrode simply needs to be in contact with the protective electrolyte to prevent rapid corrosion, therefore acting in synergy with potentially defective protective coatings.

## Results and Discussion

### *Photoelectrochemical Behavior of Silicon Photoanodes in a Protective Electrolyte*

Figure 1a compares the current density vs time behavior for  $\text{np}^+\text{-Si}(100)$  photoanodes partially coated ( $\sim 14\%$  filling fraction) with Ni islands ( $\mu\text{Ni}$ ) in 1.0 M KOH(aq) with, and without, respectively, 10 mM  $[\text{Fe}(\text{CN})_6]^{3-}$ . The photoelectrodes were held at 1.63 V vs the reversible hydrogen electrode (RHE) and were subjected to simulated, UV-filtered sunlight of  $100 \text{ mW cm}^{-2}$  illumination in 6 h intervals (“day”), followed by 18 h at open circuit in the dark (“night”). The lack of UV illumination from the ELH lamp is appropriate for proof-of-concept of the protective electrolyte approach because for unassisted water splitting Si would only be used in a tandem structure and the UV light would be filtered and absorbed by the higher band gap top cell before reaching the Si bottom cell. Representative  $\text{np}^+\text{-Si}/\mu\text{Ni}$  photoanodes exhibited  $580 \pm 20$  mV photovoltage (Fig. S1 and Table S1, ESI<sup>†</sup>). The photoanode was stable for at least twelve day/night cycles (288 h) in 10 mM  $[\text{Fe}(\text{CN})_6]^{3-}$ , 1.0 M KOH(aq) but failed at the end of the fifth day/night cycle (120 h) in 1.0 M KOH(aq). Fig. S2 (ESI<sup>†</sup>) shows that the light intensity of the lamp did not vary substantially between each day cycle during stability tests. In 10 mM  $[\text{Fe}(\text{CN})_6]^{3-}$ , 1.0 M KOH(aq) (Fig. 1b) the photoanode exhibited a fill factor of  $0.40 \pm 0.02$  and retained this value, within experimental error, for the majority of the stability test (Table S1, ESI<sup>†</sup>); the photocurrent density increased slightly, by  $< 2 \text{ mA cm}^{-2}$ ; and the photovoltage shifted

slightly positively by  $\sim 40$  mV between 120 to 288 h of operation. In contrast, in 1.0 M KOH(aq) under 1 atm O<sub>2</sub> (Fig. 1c), after 48 h the photoanode exhibited a notable decrease in fill factor from  $0.37 \pm 0.04$  to 0.27, and the electrode failed completely, with no substantial photocurrent, after 120 h of operation.

X-ray photoelectron spectroscopy (XPS) was performed before contact with the electrolyte and after one day/night cycle in both 1.0 M KOH(aq) and in the protective electrolyte (Fig. S3, ESI†). The ratios of the SiO<sub>2</sub>/Si peaks for samples prior to operation in 1.0 M KOH(aq), and for samples then immersed in 1.0 M KOH(aq) without and with 10 mM [Fe(CN)<sub>6</sub>]<sup>3-</sup>, respectively, were 0.44, 0.31, and 0.54. The presence of [Fe(CN)<sub>6</sub>]<sup>3-</sup> thus increased the amount of SiO<sub>2</sub> on the surface whereas the lack of [Fe(CN)<sub>6</sub>]<sup>3-</sup> led to etching of the initial native oxide layer as well as any subsequent anodic oxide grown during the illumination step. The ratios of the Si<sub>2</sub>O/SiO<sub>2</sub> peaks for samples immersed in KOH(aq) without and with 10 mM [Fe(CN)<sub>6</sub>]<sup>3-</sup>, respectively, were 2.75 and 1.94. The oxygen content of the SiO<sub>x</sub> film immersed in KOH(aq) was thus lower than that for the sample in KOH(aq) and [Fe(CN)<sub>6</sub>]<sup>3-</sup>, possibly due to the lack of a viable mechanism for oxide regrowth in KOH(aq) at open circuit.<sup>34</sup> Operation in either electrolyte produced a decrease in the Ni/NiO<sub>x</sub> signal, indicating that the Ni pre-electrocatalyst was converted to its NiOOH form after operation, with or without [Fe(CN)<sub>6</sub>]<sup>3-</sup> in solution.<sup>26</sup> No substantial Fe peaks were detected in 1.0 M KOH(aq) due to the relatively low surface coverage of electrocatalyst, whereas trace amounts of Fe<sub>2</sub>O<sub>3</sub> were deposited on the surface when the sample was operated in the protective electrolyte.

Fig. 2 depicts scanning-electron micrographs (SEMs) of the photoelectrodes before and after extended photoelectrochemistry under potential control in the protective electrolyte or in 1.0 M KOH(aq). After chronoamperometry in the protective electrolyte for 264 h (Fig. 2c-d),

etching of the passivating  $\text{SiO}_x$  was observed at the exposed Si surface. Beneath the  $\mu\text{Ni}$  the Si was undercut radially, leading to the formation of nanoscale pillar structures. Some delamination of  $\mu\text{Ni}$  was observed, but most of the  $\mu\text{Ni}$  remained intact after chronoamperometry, indicating some protection in the direction axial (normal to the surface) to the underlying  $\text{p}^+$ -emitter. In contrast, Fig. 2e-f show the complete failure of the photoelectrode in 1.0 M KOH(aq), with no intact  $\mu\text{Ni}$  remaining on the surface. Only the pyramid-shaped structures formed from exposed (111) Si facets remained at the center of where the  $\mu\text{Ni}$  islands were initially located. Partial pyramid formation was observed over the remainder of the surface. The loss of any appreciable photocurrent after 120 h in the corresponding chronoamperogram (Fig. 1a) is thus consistently ascribable to complete delamination of the  $\mu\text{Ni}$ .

A continuous protective layer on Si would likely lead to longer lifetimes due to limiting the exposed Si to only the regions where pinholes were present in the protective layer, but the distribution and area exposed due to possible pinholes is not generally well defined under such conditions.<sup>12, 18</sup> The  $\mu\text{m}$ -scale dimensions of the Ni catalysts is sufficient to provide protection to Si directly underneath the Ni, providing insight into possible uses of the protective electrolyte in tandem with protective layers to enhance the stability of Si photoanodes in alkaline electrolytes. In a previous study, the lifetime of Si/ $\mu\text{Ni}$  photoanodes in 1.0 M KOH(aq) was observed to be  $\sim 42$  h at open-circuit and  $\sim 240$  h under continuous illumination.<sup>26</sup> In this work, addition of an oxidizing agent,  $[\text{Fe}(\text{CN})_6]^{3-}$ , extended the lifetimes at open circuit while not hindering performance during operation, leading to device lifetimes under periodic illumination that were comparable to those exhibited by the electrode under continuous illumination.

The actual electrode lifetime depends on the formation and dissolution of the surface oxide and etching at the device junction and/or catalyst interface. In the  $\text{np}^+\text{-Si}/\mu\text{Ni}$  system, the

point of failure arises from the corrosion of the p<sup>+</sup>-emitter layer exposed to the electrolyte, followed by the undercutting of the μNi catalyst until the p<sup>+</sup>-emitter is fully etched and/or the catalyst is delaminated. As shown in Fig. 1b, this process of undercutting minimally affects the photocurrent or fill factor of the electrode, whereas a ~ 40 mV increase in overpotential occurs as some catalyst delaminates and lowers the number of active sites for OER. The lifetime of the np<sup>+</sup>-Si/μNi structure could be further increased by using a larger radius for the μNi, to retard the undercutting process. The μNi thus constitutes a partial protection layer, offering protection to the underlying Si in the axial direction but no radial protection if the Si is undercut. Larger μNi radii lead to longer lifetimes before the underlying emitter is etched, at the penalty of producing higher parasitic optical absorption by the opaque μNi precatalyst. A photoelectrode with a 14% catalyst filling fraction would have > 90% of the photocurrent exhibited by a photoanode with a 1% filling fraction, and sufficiently high filling fractions (> 10%) will minimally affect the fill factor of the device compared to photoanodes covered by a continuous metal film.<sup>26, 35</sup>

#### *Influence of Dissolved Oxygen on Photoelectrode Stability in 1.0 M KOH(aq)*

The extent to which O<sub>2</sub> passivates Si in alkaline electrolytes is an important parameter in determining the efficacy of [Fe(CN)<sub>6</sub>]<sup>3-</sup> as a passivating agent. Fig. S4 (ESI<sup>†</sup>) compares the surfaces of np<sup>+</sup>-Si/μNi photoanodes at open circuit after 24 h in 1.0 M KOH(aq) with and without, respectively, saturating the electrolyte with 1 atm of O<sub>2</sub>(g) (~ 0.2 mM dissolved). The solutions were both fully exposed to ambient air (~ 0.2 atm O<sub>2</sub>). After 24 h, the Si surface that was in contact with the 1 atm O<sub>2</sub>-saturated solution showed no visible facet-dependent etching of the Si surface or μNi delamination, whereas the Si surface that was in contact with the solution that was not continuously bubbled with O<sub>2</sub> exhibited a roughened surface with no visible μNi. Fig. S5 (ESI<sup>†</sup>) depicts a photoanode in 1.0 M KOH(aq) that had been subjected to day/night

cycles without 1 atm O<sub>2</sub> bubbling in solution. During operation in day/night cycles, the solution presumably became saturated with O<sub>2</sub> during periods of illumination, with the resulting O<sub>2</sub> thus partially stabilizing the Si surface during the dark periods. The photoanode that evolved O<sub>2</sub> for more than one cycle (24 h) lasted longer than a photoanode that had been left at open circuit, but a substantial decrease in photocurrent density (> 8 mA cm<sup>-2</sup>) and fill factor (from 0.35 to 0.18) occurred at 48 h and complete failure of the electrode occurred at 72 h of day/night operation. Bubbling O<sub>2</sub> in 1.0 M KOH(aq) extended the photoanode lifetime to 120 h, but the eventual catastrophic failure suggests that the kinetics for surface passivation via dissolved O<sub>2</sub> does not fully compete with the kinetics of Si dissolution in base.

#### *Electrochemical Potentials in a Protective Electrolyte*

Fig. S6 (ESI†) shows the potentials measured at a Pt electrode for various molar ratios of [Fe(CN)<sub>6</sub>]<sup>3-</sup> to [Fe(CN)<sub>6</sub>]<sup>4-</sup> in either 1.0 M KOH(aq) or deionized water. The measured potentials ranged from ~ 0.3 to ~ 0.6 V vs the normal hydrogen electrode (NHE), comparable to  $E^0(\text{O}_2/\text{OH}^-) = 0.401 \text{ V vs NHE at pH 14}$  and consistent with Nernstian behavior. The potential of [Fe(CN)<sub>6</sub>]<sup>3-/4-</sup> depends on the ionic strength,<sup>36</sup> and as expected exhibited a ~ 100 mV positive shift in 1.0 M KOH(aq) compared to in deionized H<sub>2</sub>O. The passivation potential of Si in 1.0 M KOH(aq) is ~ 0.5 vs RHE (~ -0.3 V vs NHE at pH 14),<sup>25, 29</sup> so either holding a Si electrode passively in [Fe(CN)<sub>6</sub>]<sup>3-/4-</sup> or at potentials for water oxidation is expected to produce a sufficiently positive potential to oxidize the Si surface.

The behavior of Si electrodes in the dark was elucidated further by investigating the open-circuit potential ( $E_{\text{oc}}$ ) under various conditions. Fig. S7 (ESI†) compares the  $E_{\text{oc}}$  values measured over 18 h cycles for p<sup>+</sup>-Si electrodes with and without μNi, in contact with O<sub>2</sub>-saturated 1.0 M KOH(aq) with or without [Fe(CN)<sub>6</sub>]<sup>3-</sup>. Each cycle was preceded by 6 h at 1.58 V

vs RHE during which time the Si surface passivated and produced  $\text{SiO}_x$ .<sup>24</sup> In 1.0 M KOH(aq),  $E_{oc}$  after each cycle of potential control was  $-0.07 \pm 0.01$  V for  $\text{p}^+$ -Si and was  $0.41 \pm 0.07$  V for  $\text{p}^+$ -Si/ $\mu\text{Ni}$ . After  $\sim 1$  h at  $E_{oc}$  for  $\text{p}^+$ -Si in 1.0 M KOH(aq),  $E_{oc}$  was  $\sim 0.1$  V before settling at  $-0.07$  V, which corresponds to removal of the surface  $\text{SiO}_x$ , followed by etching of the underlying Si.<sup>30</sup> Along with relatively steady, positive potentials across all four cycles effected by the equilibration of  $\mu\text{Ni}$  with electrolyte, the  $\text{p}^+$ -Si/ $\mu\text{Ni}$  electrode in 1.0 M KOH(aq) did not exhibit this decrease in  $E_{oc}$  to  $-0.07$  V, indicating that Ni remained intact on the Si surface. In 1.0 M KOH(aq) containing  $[\text{Fe}(\text{CN})_6]^{3-}$ ,  $E_{oc}$  was  $0.99 \pm 0.02$  V vs RHE for  $\text{p}^+$ -Si and was  $1.32 \pm 0.03$  V for  $\text{p}^+$ -Si/ $\mu\text{Ni}$ . The potential of 1.43 V vs RHE for  $\text{p}^+$ -Si/ $\mu\text{Ni}$  was comparable to that of a Pt electrode in the protective electrolyte, suggesting that the surface potential of the  $\text{p}^+$ -Si/ $\mu\text{Ni}$  electrode equilibrated near the Nernstian potential of  $[\text{Fe}(\text{CN})_6]^{3-/4-}$  at open circuit. The  $\text{p}^+$ -Si potential was comparatively less positive and complicated by the lack of metallic contact. Regardless of the presence of Ni, compared to in 1.0 M KOH(aq) the protective electrolyte increased  $E_{oc}$  to potentials that were well above ( $> 0.5$  V) the passivation potential of Si.

#### *Etch Rates of Si/SiO<sub>x</sub>*

Various descriptions of the Si and  $\text{SiO}_x$  corrosion process in alkaline electrolyte have been provided.<sup>25, 32, 37-39</sup> Experimental evidence indicates that reduction of  $[\text{Fe}(\text{CN})_6]^{3-}$  on p-Si anodes in alkaline electrolytes proceeds via surface intermediates,<sup>33</sup> suggesting that the interaction of an oxidant with reaction intermediates plays a key role in determining oxide formation. Figure S8 (ESI†) provides one possible scheme in which the  $\text{SiO}_x$  growth and dissolution is preceded by hole injection via positive bias or  $[\text{Fe}(\text{CN})_6]^{3-}$ , whereas Si dissolution occurs in the absence of injected holes.<sup>37</sup> The relative rates of Si and  $\text{SiO}_x$  dissolution are thus critical towards stabilizing Si photoanodes.

Fig. 3 shows the etch rate of p<sup>+</sup>-Si in 1.0 M KOH(aq) without or with varying concentrations of [Fe(CN)<sub>6</sub>]<sup>3-</sup>, as determined by measuring the height differences between a protected Si surface and a Si surface exposed to etching (See Fig. S9, ESI† for experimental details). During evaluation of the etch rate, the solution was not saturated with O<sub>2</sub>. Si(111) is the slowest etching facet of Si, leading to exposed Si(111) facets determining the etch pit morphology of both Si(100) and Si(111) in KOH(aq) (Fig. S10, ESI†).<sup>40</sup> Conversely, Si(100) etched in the protective electrolyte produced flat profiles with no facet dependence, indicating that the etching process was based on SiO<sub>x</sub> formation and dissolution rather than direct Si dissolution. The lack of a facet dependence moreover implies that SiO<sub>x</sub> covered the entirety of the Si surface. Si electrode areas in the cm<sup>2</sup>-scale (tested up to 0.88 cm<sup>2</sup>) yielded < 2% differences in etch depth when sampling 15 random points on an electrode, underscoring the uniformity and scalability of the SiO<sub>x</sub> growth and dissolution process. Fig. 3 and Table S2 (ESI†) compare the etch rates,  $R_{Si}$ , of various Si samples. In the protective electrolyte, Si(100) and Si(111) displayed etch rates of 1.8±0.1 and 1.7±0.1 nm h<sup>-1</sup>, respectively, whereas in 1.0 M KOH(aq), Si(100) and Si(111) etched at 330±20 and 84±6 nm h<sup>-1</sup>, respectively. Holding the Si at 1.63 V vs RHE in either the protective electrolyte or in 1.0 M KOH(aq) produced etch rates of 2.7±0.1 and 2.9±0.1 nm h<sup>-1</sup>, respectively. Anodized Si oxide is more porous than thermal Si oxides or bulk silica, leading to more surface area exposed for chemical attack by the alkaline electrolyte.<sup>41</sup> The lower etch rates of Si in protective electrolyte at  $E_{oc}$  suggest that the oxide formed by the reduction of [Fe(CN)<sub>6</sub>]<sup>3-</sup> could be comparatively more compact than the oxide in anodized films. The etch rate experiments presented in Fig. 3a further support the hypothesis that O<sub>2</sub> is not needed for [Fe(CN)<sub>6</sub>]<sup>3-</sup> to oxidize the surface, because the etch rates were measured in

the absence of bubbled  $O_2(g)$  and the electrode still displayed consistent and conformal oxidation of Si in the presence of  $[Fe(CN)_6]^{3-}$ .

Fig. 3b shows a positive correlation between the etch rate of Si at  $E_{oc}$  in 1.0 M KOH(aq) and the concentration of  $[Fe(CN)_6]^{3-}$ , with 100 mM and 0.5 mM  $[Fe(CN)_6]^{3-}$  having etch rates of  $2.1 \pm 0.1$  and  $1.2 \pm 0.1$  nm  $h^{-1}$ , respectively. However, mass transfer limitations likely occur at sufficiently low concentrations of  $[Fe(CN)_6]^{3-}$  ( $< 0.5$  mM), with Si dissolution outcompeting the  $[Fe(CN)_6]^{3-}$  flux to the surface, leading to unhindered etching. Fig. S11 (ESI†) shows that  $p^+$ -Si(100) subjected to concentrations of  $[Fe(CN)_6]^{3-} > 0.5$  mM in 1.0 M KOH(aq) had surface roughness values ( $R_a$ ) of  $\sim 0.2$  nm that were essentially independent of the  $[Fe(CN)_6]^{3-}$  concentration.  $p^+$ -Si(100) exposed to 0.5 mM  $[Fe(CN)_6]^{3-}$  in 1.0 M KOH(aq) had  $R_a = 2.12$  nm with no exposed Si(111) facets. The rougher surface morphology at 0.5 mM  $[Fe(CN)_6]^{3-}$  concentration compared to higher oxidant concentrations could be a result of locally varying etch rates as a direct consequence of mass transfer limitations. Fig. S12 (ESI†) shows the Si 2p XPS data indicating mutually similar oxide compositions and oxidation states at various concentrations of oxidant, with the  $SiO_2/Si$  peak ratios being 0.29, 0.23, 0.24, or 0.30 for Si exposed to 1.0 M KOH(aq) and 0.5, 1.0, 10, or 100 mM  $[Fe(CN)_6]^{3-}$ , respectively. For concentrations between 1-100 mM  $[Fe(CN)_6]^{3-}$  the  $SiO_2$  content increased slightly for samples subjected to increasing  $[Fe(CN)_6]^{3-}$  concentration, whereas at the 0.5 mM  $[Fe(CN)_6]^{3-}$  threshold the  $SiO_2$  content did not follow this trend due to the slightly higher surface area available for oxidation as a result of the rougher surface. Above the 0.5 mM threshold concentration of  $[Fe(CN)_6]^{3-}$ , the monotonically increasing etch rate with  $[Fe(CN)_6]^{3-}$  concentration suggests that  $[Fe(CN)]^{3-}$  could facilitate  $SiO_x$  dissolution during etching in addition to conformal oxidation of Si to  $SiO_x$ . Consequently, the lowest etch rate occurred around 0.5 mM  $[Fe(CN)_6]^{3-}$ , indicating a

trade-off between having sufficient  $[\text{Fe}(\text{CN})_6]^{3-}$  to react with Si to  $\text{SiO}_x$  and the presence of  $[\text{Fe}(\text{CN})_6]^{3-}$  facilitating dissolution of  $\text{SiO}_x$ . Although the 10 mM  $[\text{Fe}(\text{CN})_6]^{3-}$  used in stability tests (Fig. 1) was not the optimal concentration in terms of minimizing the  $\text{SiO}_x$  etch rate, it was sufficient to prevent the concentration from reaching the 0.5 mM threshold due to residual  $[\text{Fe}(\text{CN})_6]^{3-}$  photodegradation over the > 200 h run. The process by which  $[\text{Fe}(\text{CN})_6]^{3-}$  facilitates  $\text{SiO}_x$  dissolution requires further elucidation and does not affect the primary findings herein that a protective electrolyte can be utilized to protect Si photoanodes in KOH at open circuit, because the difference of a factor of < 2 in etch rate between 0.5 mM and 100 mM  $[\text{Fe}(\text{CN})_6]^{3-}$  is minor when compared to the Si etch rate in 1.0 M KOH(aq) without  $[\text{Fe}(\text{CN})_6]^{3-}$ .

The presence of Ni on the Si surface could also impact the etch rate of  $\text{SiO}_x$  in the protective electrolyte. Based on the cross-sectional view of an etched  $\text{np}^+\text{-Si}/\mu\text{Ni}$  electrode after 264 h (Fig. 2d) and assuming that the observed catalyst delamination occurred near the end of testing, the depth etched in the direction normal to the planar surface was  $0.86 \pm 0.02 \mu\text{m}$ , corresponding to an etch rate of  $3.3 \pm 0.1 \text{ nm h}^{-1}$ . Similarly, the radial etching that led to undercutting of  $2.83 \pm 0.05 \mu\text{m}$  diameter  $\mu\text{Ni}$  corresponded to  $1.03 \pm 0.08 \mu\text{m}$  of  $\text{Si}/\text{SiO}_x$  etched, or  $R_{\text{Si}} = 3.9 \pm 0.3 \text{ nm h}^{-1}$ . Compared to a value of  $R_{\text{Si}} = 1.8 \pm 0.1 \text{ nm h}^{-1}$  for  $\text{Si}/\text{SiO}_x$  alone, these higher etch rates of  $\text{Si}/\text{SiO}_x$  in close proximity to  $\mu\text{Ni}$  suggest that the Ni may assist in the  $\text{Si}/\text{SiO}_x$  etching process. The non-zero etch rate of the oxide in alkaline media will ultimately limit the stability of Si photoanodes even in the protective electrolyte, with the failure time depending on the exact thickness of the absorber, emitter layer (if any), and propensity of pitting corrosion to laterally undercut and delaminate the  $\mu\text{Ni}$  electrocatalyst islands.

*Faradaic Efficiency and Catalyst Activity in a Protective Electrolyte*

Fig. 4 shows faradaic efficiency and OER activity of p<sup>+</sup>-Si/(μ)Ni in 1.0 M KOH(aq) with and without [Fe(CN)<sub>6</sub>]<sup>3-</sup>. Illuminated Si/Ni photoanodes passivate in KOH at potentials relevant to OER,<sup>42, 43</sup> and consequently exhibit near unity faradaic efficiencies for O<sub>2</sub> production under illumination.<sup>44</sup> Hence the behavior of p<sup>+</sup>-Si anodes in the dark was investigated to determine the effects of [Fe(CN)<sub>6</sub>]<sup>3-</sup> on the dark electrode stability of Si and to confirm that the current density associated with oxidation of the trace amounts of [Fe(CN)<sub>6</sub>]<sup>4-</sup> formed by oxidation of the Si to protect the electrode from dissolution in KOH(aq) did not substantially affect the faradaic efficiency for O<sub>2</sub> production. Prior to electrochemistry, electrodes were cycled at positive potentials in 1.0 M KOH(aq) to incorporate Fe impurities into the Ni precatalyst and form NiFeOOH.<sup>9</sup> Based on the amount of O<sub>2</sub>(g) evolved and the charge passed at a constant 40 mA cm<sup>-2</sup> current density, the p<sup>+</sup>-Si/Ni film electrode exhibited > 97% faradaic efficiency (Fig. 4a) for the duration of the measurement regardless of the presence of [Fe(CN)<sub>6</sub>]<sup>3-</sup> in solution. The p<sup>+</sup>-Si/μNi anode similarly had > 96% faradaic efficiency when passing charge and measuring O<sub>2</sub> both after initial contact with the protective electrolyte and after resting for 45 h at open circuit, signifying that the oxidation of exposed Si was a negligible fraction of the overall charge passed. The near unity faradaic efficiency in 1.0 M KOH(aq) and in the protective electrolyte can be understood by the order of magnitude for the current associated with either anodic passivation or [Fe(CN)<sub>6</sub>]<sup>3-</sup>. For an etch rate of 2.7 nm h<sup>-1</sup> of an anodic oxide in protective electrolyte, ~ 1.3 μA cm<sup>-2</sup> (See SI† for calculations) is expected from oxidation of Si, comprising ~ 0.003% of the total current passed in this experiment. Oxidation of Si in the dark at open circuit similarly leads to a small rate of reduction of [Fe(CN)<sub>6</sub>]<sup>3-</sup>, of 8.8x10<sup>-12</sup> mol s<sup>-1</sup> cm<sup>-2</sup> compared to 7.8x10<sup>-8</sup> mol s<sup>-1</sup> cm<sup>-2</sup> of O<sub>2</sub>(g) generated assuming 30 mA cm<sup>-2</sup> of photocurrent. Consequently, the moles of [Fe(CN)<sub>6</sub>]<sup>4-</sup> produced in 88 h in the dark would produce ~ 1% of the moles of O<sub>2</sub>(g) generated in

1 h under illumination. The oxidation of  $[\text{Fe}(\text{CN})_6]^{4-}$  back to  $[\text{Fe}(\text{CN})_6]^{3-}$  under potential control would thus be negligibly small compared to the current associated with the OER, consistent with the measured faradaic efficiency found in Fig. 4a.

In contrast to cycling between light with positive bias and dark at open circuit in Fig. 1 and 2, the activated  $\text{p}^+\text{-Si/Ni}$  electrode in Fig. 4b was galvanostatically held at  $10 \text{ mA cm}^{-2}$  continuously for 96 h. Under continuous operation, any exposed Si forms an oxide layer due to the applied positive bias.<sup>26</sup> The electrode exhibited stable overpotentials for > 96 h in both 1.0 M KOH(aq) and in the protective electrolyte, with nearly identical average overpotentials of  $336 \pm 4$  and  $340 \pm 4$  mV, respectively (Fig. 4b). As expected for a one-electron redox species,  $[\text{Fe}(\text{CN})_6]^{3-}$  did not catalyze the four-hole oxidation of water to  $\text{O}_2(\text{g})$ , as evidenced by the mutually similar overpotentials of both systems. Cyclic voltammetric measurements (Fig. 4c) before and after galvanostatic control, respectively, indicated that the electrodes did not exhibit any appreciable change in resistance. These results suggest that  $[\text{Fe}(\text{CN})_6]^{3-}$  minimally affected the faradaic efficiency towards OER or the electrocatalytic behavior of the NiFeOOH catalyst.

#### *Stability of $[\text{Fe}(\text{CN})_6]^{3-}$ as a protective electrolyte*

The concentrations of  $[\text{Fe}(\text{CN})_6]^{3-}$  and  $[\text{Fe}(\text{CN})_6]^{4-}$  were monitored using UV-vis spectroscopy through a correlation between the 420 nm and 260 nm absorption peaks.<sup>45</sup> Fig. S13 (ESI†) shows the spectra for solutions of 1 mM  $[\text{Fe}(\text{CN})_6]^{3-}$  and 0.1 M KOH(aq) in the dark (Fig. S13a, ESI†) or under illumination with either a red (627 nm) LED (Fig. S13b, ESI†) or an ELH-type W-halogen lamp with a 400 nm long pass filter (Fig. S13c, ESI†).  $[\text{Fe}(\text{CN})_6]^{3-}$  decomposes under UV-light,<sup>46</sup> so a UV long pass filter was used to minimize this decomposition process. Nevertheless, the solution absorbs strongly below 480 nm, lowering the  $[\text{Fe}(\text{CN})_6]^{3-}$  concentration from 1.0 mM to 0.09 mM over 120 h when subjected to visible light (Fig. S13d,

ESI†). This decrease in concentration can be accounted for by the light-driven decomposition to  $\text{Fe}_2\text{O}_3$  as well as reduction to  $[\text{Fe}(\text{CN})_6]^{4-}$ , whose concentration increased from  $\sim 0$  mM to 0.66 mM within the same timeframe.<sup>47</sup>  $\text{Fe}_2\text{O}_3$  was observed as a red-orange colored precipitate that was verified to be  $\text{Fe}_2\text{O}_3$  by XPS (Fig. S14, ESI†). Under dark conditions or red LED illumination, the  $[\text{Fe}(\text{CN})_6]^{3-}$  remained stable in  $\text{KOH}(\text{aq}) > 120$  h without any notable decrease in the absorption peaks corresponding to  $[\text{Fe}(\text{CN})_6]^{3-}$ , and no precipitate was observed after the solution was centrifuged.

Fig. S15a (ESI†) shows a chronoamperometric stability run for an  $\text{np}^+\text{-Si}(100)/\mu\text{Ni}$  electrode in 1.0 M  $\text{KOH}(\text{aq})$  and 10 mM  $[\text{Fe}(\text{CN})_6]^{3-}$  that was subjected to  $100 \text{ mW cm}^{-2}$  illumination from a Xe arc lamp with an AM 1.5 filter during the day cycles. In contrast to Fig. 1a, no UV filter was placed between the electrode and light source, leading to accelerated decomposition of  $[\text{Fe}(\text{CN})_6]^{3-}$ . At the end of each 24 h day/night cycle, the electrolyte was replaced with fresh electrolyte to ensure the presence of sufficient  $[\text{Fe}(\text{CN})_6]^{3-}$  to oxidize Si at open circuit. The temporary drops in photocurrent each day was consistently attributed to parasitic absorption by the  $\text{Fe}_2\text{O}_3$  precipitate that formed and was dispersed within the solution, whereas later erratic behavior is likely due to adsorption and desorption of precipitate on the electrode surface. Fig. S15b (ESI†) shows that although the light limiting current was mostly stable after the electrolyte was replaced and a majority of the  $\text{Fe}_2\text{O}_3$  was removed (but not all) after each day, more pronounced changes to the onset potential ( $\sim +100$  mV) and fill factor (from 0.37 to 0.16) were observed relative to an electrochemical cell that was not subjected to UV light (Fig. 1b). The negligible dark current in Fig. S15b (ESI†) suggests that the bare Si was not corroding rapidly throughout the stability test. Fig. S16 (ESI†) shows that the increasing electrode resistance can be attributed to accelerated delamination of  $\mu\text{Ni}$  throughout most of the

electrode compared to Fig. 2c. The  $\mu\text{Ni}$  located near the edges of the electrode remained mostly intact (Fig. S16b, ESI†). The electrode behavior could thus be attributed to the accumulation of dispersed  $\text{Fe}_2\text{O}_3$  precipitate, which acted as an abrasive that facilitated mechanical delamination of  $\mu\text{Ni}$  of the exposed electrode surface. In contrast,  $\mu\text{Ni}$  near the electrode edges was protected by the surrounding epoxy that protruded over the surface.

$[\text{Fe}(\text{CN})_6]^{3-}$  is stable under red light and absorbs light only under  $\sim 480$  nm, so managing the wavelength range of light entering the anolyte compartment serves to both stabilize the  $[\text{Fe}(\text{CN})_6]^{3-}$  and minimize its parasitic absorption when under illumination. Although filtering all light absorbed by  $[\text{Fe}(\text{CN})_6]^{3-}$  is one way to stabilize this species, such an approach is undesirable in practice because large portions of the solar spectrum would not be utilized, hindering the amount of photocurrent that could be obtained. Achieving stable operation with  $[\text{Fe}(\text{CN})_6]^{3-}$  in sunlight is realizable in a tandem cell configuration with incident light going through the catholyte followed sequentially by light going through the anolyte. The small band gap of Si precludes the semiconductor alone from achieving the  $\sim 1.7$  V necessary to spontaneously split water,<sup>48</sup> so integrated tandem devices with a wide band gap semiconductor as the top cell and Si as the bottom cell have been proposed.<sup>2, 3, 49</sup> In an optimally configured tandem cell, each half-cell absorbs half of incoming photons with higher energy photons being more readily absorbed by the top, wider band gap semiconductor. One proposed device architecture that satisfies this configuration uses semiconductor nano- and microwire arrays embedded in a membrane, which maximizes high-energy photons collected by the top cell and minimizes the path length of low energy photons in the anolyte.<sup>50, 51</sup> Lower energy photons that pass through the catholyte can be harvested by the Si bottom cell, subsequently minimizing any parasitic absorption caused by the  $[\text{Fe}(\text{CN})_6]^{3-}$ .

## Conclusions

The studies conducted herein emphasize the importance of active redox species at the semiconductor/electrolyte interface for the development of stable photoelectrodes. The prevailing strategy for stabilizing electrodes in corrosive electrolytes has involved coatings that are impermeable to electrolytes but allow light and photogenerated charge to be transmitted. This strategy has resulted in a substantial improvement in photoelectrode stability, particularly for Si photoanodes. However, protected photoanodes often contain defects on the metal oxide film (pinholes) that allow the electrolyte to react with the photoelectrode, leading to eventual device failure.<sup>18, 29, 52</sup> The work presented herein demonstrates that a protective electrolyte is conceptually different than a protective film, and allows the photoelectrode to be protected when exposed to a corrosive electrolyte. Protective electrolytes can be utilized in conjunction with protective coatings and subsequently allow for increased tolerance to physical defects in protective films, constituting an attractive property for device systems that need to be scalable.

The protective electrolyte self-healing strategy can be generalized to other oxidizing agents that have a potential that allows for spontaneous reaction with the photoelectrode to form a passivating layer. The oxidizing agents must be stable in the electrolyte, should have minimal parasitic light absorption, and must have fast kinetics for both oxidation and reduction. For Si photoanodes, oxidizing agents like  $\text{MnO}_4^-$  and  $\text{CrO}_4^{2-}$  may be considered, however they have been shown to adsorb onto  $\text{SiO}_x$  and hinder oxide growth, leading to higher oxide dissolution rates.<sup>37</sup> Furthermore,  $\text{MnO}_4^-$  absorbs strongly in the visible range whereas  $\text{CrO}_4^{2-}$  is a carcinogen, posing a potential health risk when considering scaled-up systems.<sup>37, 53</sup> Although  $\text{O}_2$  is colorless, non-toxic, and abundant from both ambient air and as an evolved product of water splitting, the

slow kinetics for O<sub>2</sub> reduction prevent it from being an adequate redox species for a protective electrolyte.

In summary, addition of [Fe(CN)<sub>6</sub>]<sup>3-</sup> to 1.0 M KOH(aq) extends the lifetime of Si photoanodes patterned with Ni catalyst islands to  $\geq 288$  h under simulated day/night cycles, equivalent to 12 days of operation. The Si surface was oxidized by a SiO<sub>x</sub> layer formed via either by anodic current supplied from photogenerated holes or by [Fe(CN)<sub>6</sub>]<sup>3-</sup>. The presence of [Fe(CN)<sub>6</sub>]<sup>3-</sup> did not hinder the catalytic activity of NiFeOOH or the faradaic efficiency for the OER. In the protective electrolyte, the Si(100) etch rate was  $> 180$  times slower, and independent of the facet, compared to the behavior in 1.0 M KOH(aq) alone. These findings show that the spontaneous passivation of exposed Si that allows for long ( $> 100$  h) device lifetimes under conditions for OER can also be achieved in the dark at open circuit, marking an important step towards operation of Si photoanodes under realistic varying insolation conditions. Protective electrolytes like [Fe(CN)<sub>6</sub>]<sup>3-</sup> that enable self-healing of photoelectrodes could be utilized in conjunction with protective layers to further extend device lifetimes.

### **Acknowledgments**

This work was supported through the Office of Science of the U.S. Department of Energy (DOE) under award no. DE-SC0004993 to the Joint Center for Artificial Photosynthesis, a DOE Energy Innovation Hub. Research was in part carried out at the Molecular Materials Resource Center of the Beckman Institute. We thank M. H. Richter for assistance in automating day/night cycles.

## Figures:

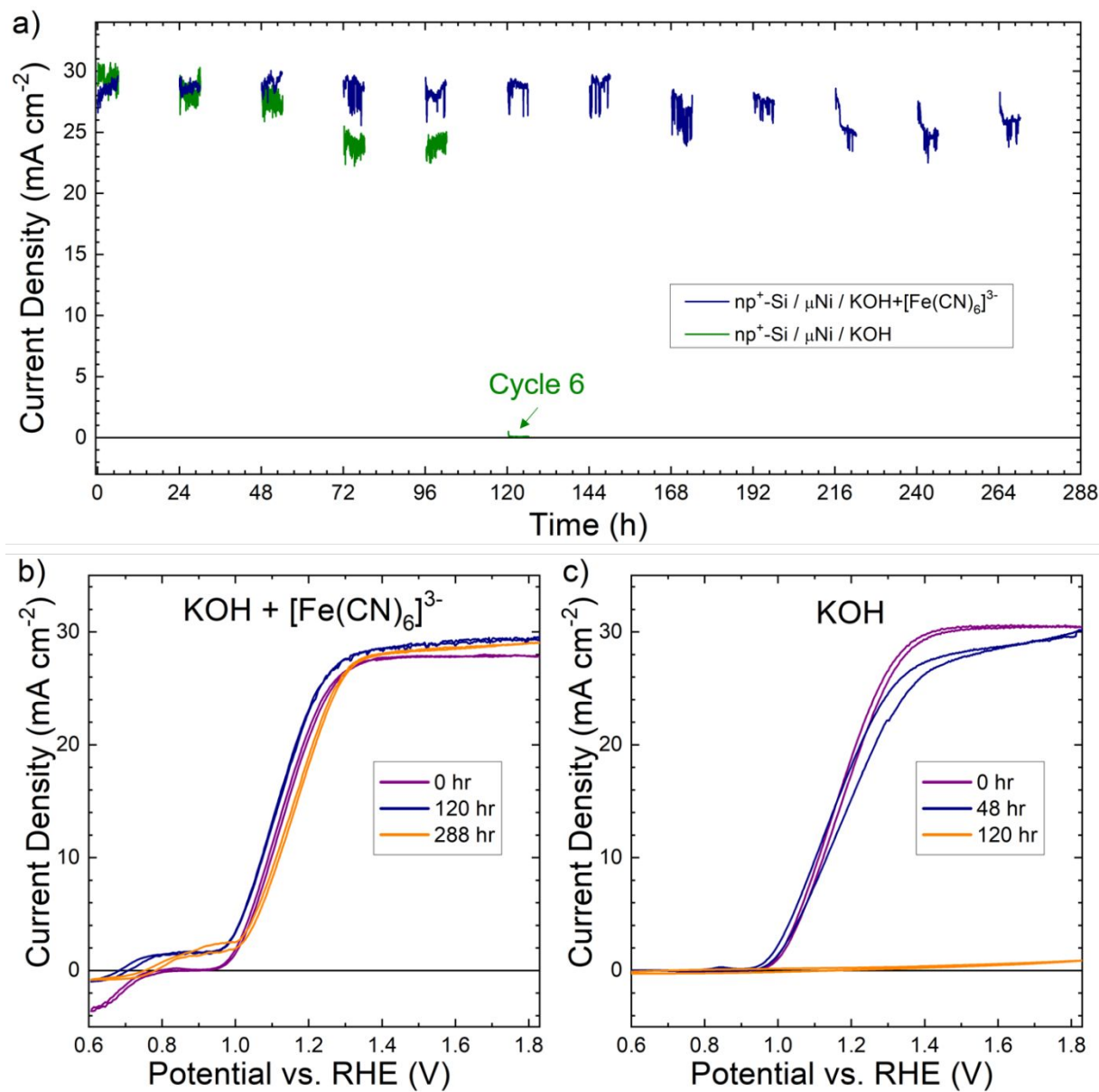


**Figure 1.** Chronoamperometric stability and performance of  $\text{np}^+\text{-Si}(100)/\mu\text{Ni}$  electrodes in 1.0 M  $\text{KOH}(\text{aq})$  with and without, respectively, 10 mM  $[\text{Fe}(\text{CN})_6]^{3-}$ . (a) Stability in  $\text{KOH}(\text{aq})$  (blue) or in  $[\text{Fe}(\text{CN})_6]^{3-}$ ,  $\text{KOH}(\text{aq})$  (green). Chronoamperometric data were taken for 6 h intervals at 1.63 V vs RHE under  $100 \text{ mW cm}^{-2}$  illumination provided by an ELH-type W-halogen lamp with a long pass filter, followed by 18 h in the dark at open circuit. Cyclic voltammograms of  $\text{np}^+\text{-Si}(100)/\mu\text{Ni}$  electrodes in (b) 1.0 M  $\text{KOH}(\text{aq})$  and 10 mM  $[\text{Fe}(\text{CN})_6]^{3-}$  and (c) 1.0 M  $\text{KOH}(\text{aq})$

collected periodically during the chronoamperometric stability test. The scan rate of the cyclic voltammograms is  $100 \text{ mV s}^{-1}$ .

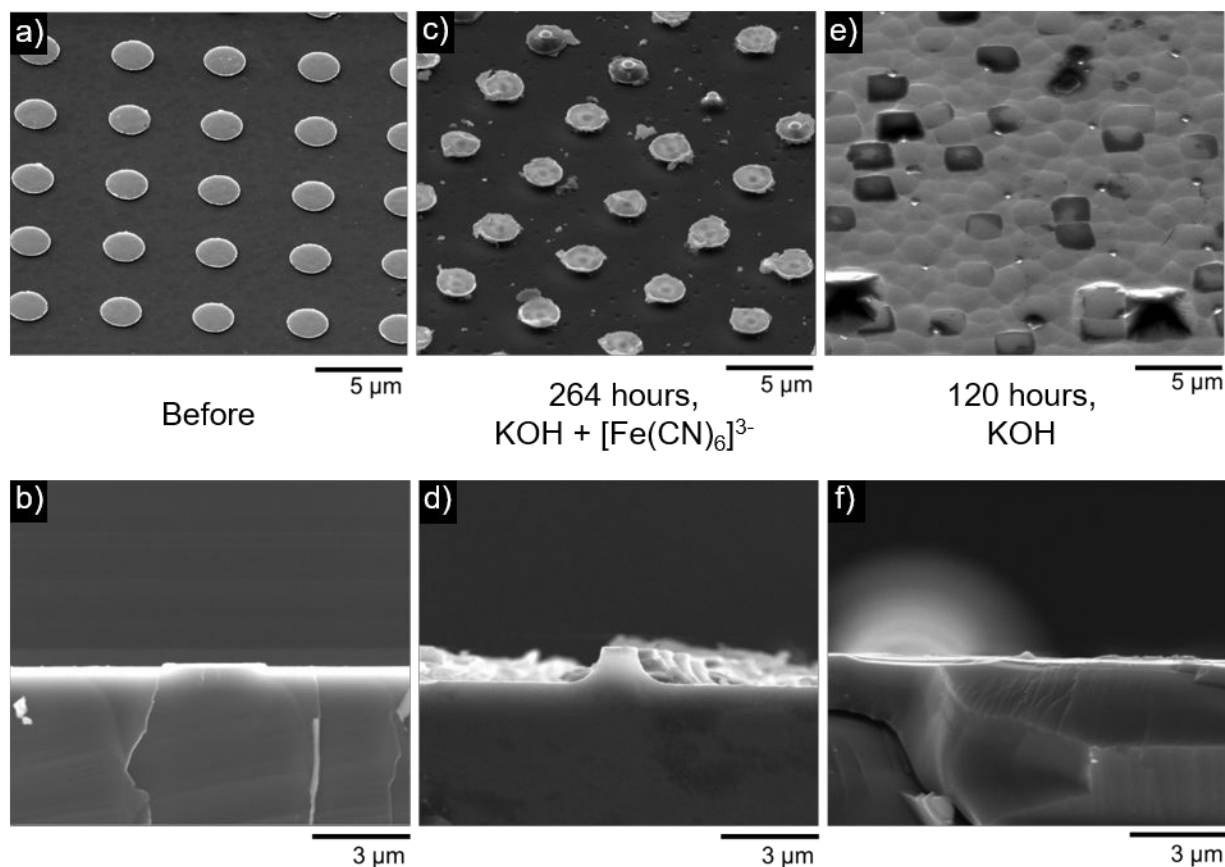


**Figure 2.** Scanning-electron micrographs of  $\text{np}^+\text{-Si}(100)/\mu\text{Ni}$  electrodes. (a-b) Top-down (a) and cross section (b) of electrodes before day/night cycling. (c-d) Top-down (c) and cross-section (d) after 264 h in 10 mM  $[\text{Fe}(\text{CN})_6]^{3-}$ , 1.0 M KOH(aq). (e-f) Top-down (e) and cross-section (f) after 133 h in 1.0 M KOH(aq).

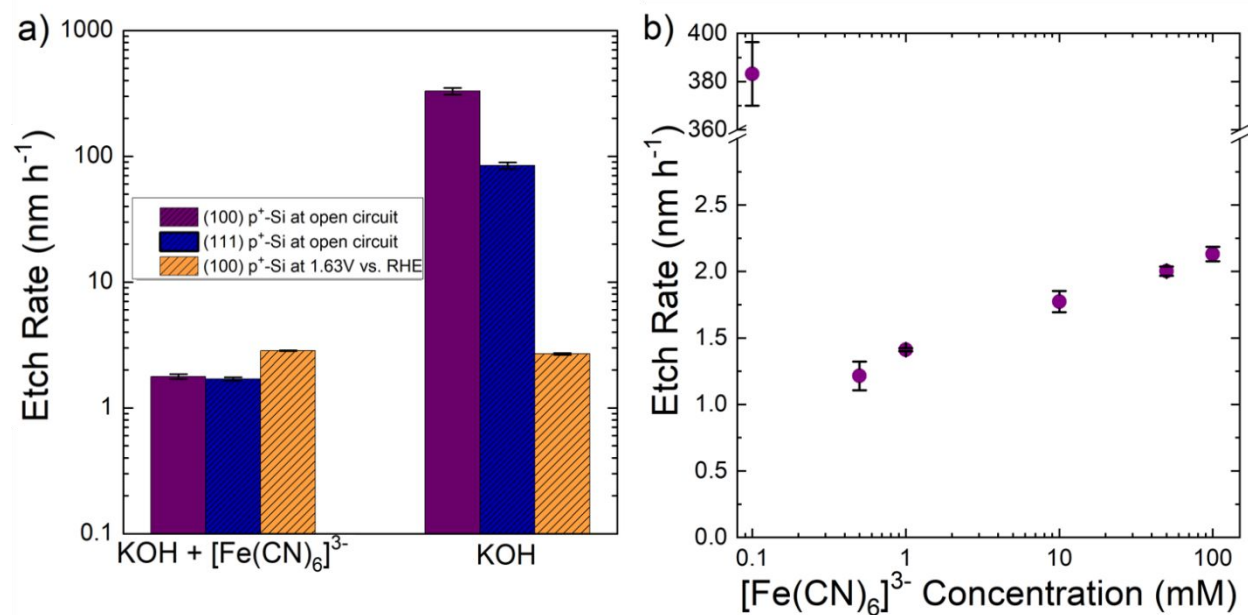


**Figure 3.** Influence of  $[\text{Fe}(\text{CN})_6]^{3-}$  on the etch rate of p<sup>+</sup>-Si in 1.0 M KOH(aq). (a) Comparison of Si(100) at open circuit (purple), Si(111) at open circuit (blue), and Si(100) at 1.63 V vs RHE (orange) in either the protective electrolyte (10 mM  $[\text{Fe}(\text{CN})_6]^{3-}$ , 1.0 M KOH(aq)) or in 1.0 M KOH(aq). (b) Dependence of the Si(100) etch rate on  $[\text{Fe}(\text{CN})_6]^{3-}$  concentration in 1.0 M KOH(aq) at open circuit.

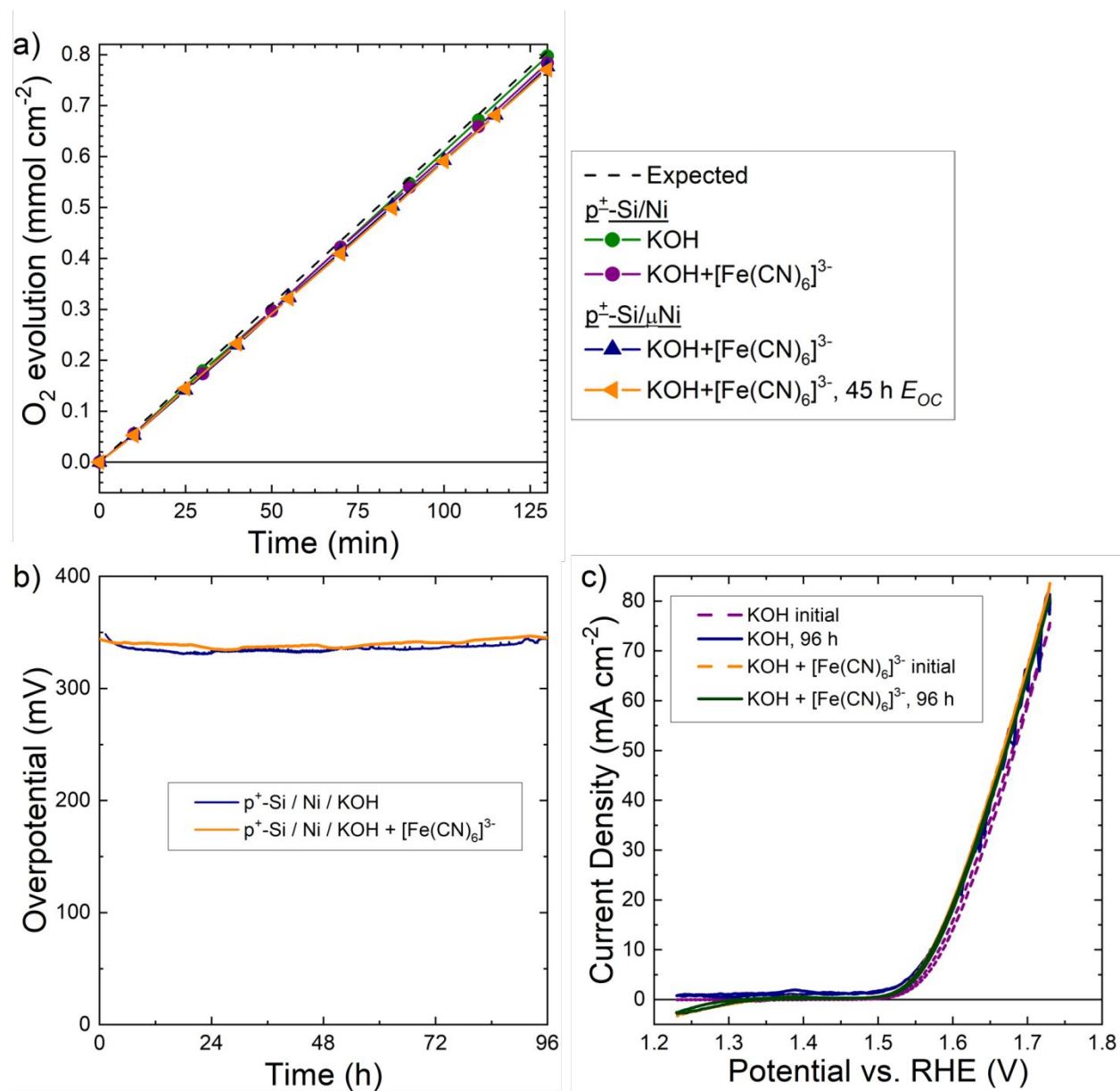


**Figure 4.** Catalytic performance of  $p^+$ -Si/ $\mu$ Ni electrodes for the OER in 1.0 M KOH(aq) with or without 10 mM ferricyanide. (a) Faradaic efficiency measurements via an eudiometer for  $p^+$ -Si/ $\mu$ Ni (triangle) and  $p^+$ -Si/Ni film (circle) electrodes held galvanostatically at 40  $mA\ cm^{-2}$ . Charge passed and  $O_2$  measurement began after the electrodes were in contact with the solution and were repeated for the  $p^+$ -Si/ $\mu$ Ni electrode after resting at open circuit ( $E_{OC}$ ) for an additional 45 h. (b) Chronopotentiometry at 10  $mA\ cm^{-2}$  of a  $p^+$ -Si/Ni film electrode in KOH(aq) (blue) or

in  $[\text{Fe}(\text{CN})_6]^{3-}$ ,  $\text{KOH}(\text{aq})$  (orange). (c) Cyclic voltammetry at  $10 \text{ mV s}^{-1}$  before and after chronopotentiometry. The  $\text{p}^+\text{-Si/Ni}$  film electrodes were prepared by depositing 100 nm of Ni onto  $\text{p}^+\text{-Si}$  and activating the electrodes in 1.0 M  $\text{KOH}(\text{aq})$  with 20 cycles between 0.53 V and 1.83 V vs RHE at  $40 \text{ mV s}^{-1}$ , to incorporate Fe impurities from the electrolyte and to form  $\text{NiFeOOH}$ .<sup>9</sup>

## References

1. N. S. Lewis, *Science*, 2016, **351**, aad1920.
2. S. Hu, C. Xiang, S. Haussener, A. D. Berger and N. S. Lewis, *Energy & Environmental Science*, 2013, **6**, 2984-2993.
3. M. R. Shaner, K. T. Fountaine, S. Ardo, R. H. Coridan, H. A. Atwater and N. S. Lewis, *Energy & Environmental Science*, 2014, **7**, 779-790.
4. A. G. Aberle, S. Glunz and W. Warta, *Journal of Applied Physics*, 1992, **71**, 4422-4431.
5. K. Sun, X. Pang, S. Shen, X. Qian, J. S. Cheung and D. Wang, *Nano Letters*, 2013, **13**, 2064-2072.
6. M. J. Kenney, M. Gong, Y. Li, J. Z. Wu, J. Feng, M. Lanza and H. Dai, *Science*, 2013, **342**, 836-840.
7. P. Xu, J. Feng, T. Fang, X. Zhao, Z. Li and Z. Zou, *RSC Advances*, 2016, **6**, 9905-9910.
8. C. C. L. McCrory, S. Jung, J. C. Peters and T. F. Jaramillo, *Journal of the American Chemical Society*, 2013, **135**, 16977-16987.
9. L. Trotochaud, S. L. Young, J. K. Ranney and S. W. Boettcher, *Journal of the American Chemical Society*, 2014, **136**, 6744-6753.
10. B. S. Yeo and A. T. Bell, *Journal of the American Chemical Society*, 2011, **133**, 5587-5593.
11. D. A. Corrigan and R. M. Bendert, *Journal of The Electrochemical Society*, 1989, **136**, 723-728.
12. S. Hu, M. R. Shaner, J. A. Beardslee, M. Lichterman, B. S. Brunschwig and N. S. Lewis, *Science*, 2014, **344**, 1005-1009.
13. I. A. Moreno-Hernandez, B. S. Brunschwig and N. S. Lewis, *Advanced Energy Materials*, 2018, **8**, 1801155.
14. K. Sun, F. H. Saadi, M. F. Lichterman, W. G. Hale, H. P. Wang, X. Zhou, N. T. Plymale, S. T. Omelchenko, J. H. He, K. M. Papadantonakis, B. S. Brunschwig and N. S. Lewis, *Proc Natl Acad Sci U S A*, 2015, **112**, 3612-3617.
15. X. Zhou, R. Liu, K. Sun, K. M. Papadantonakis, B. S. Brunschwig and N. S. Lewis, *Energy & Environmental Science*, 2016, **9**, 892-897.
16. Y. W. Chen, J. D. Prange, S. Dühnen, Y. Park, M. Gunji, C. E. D. Chidsey and P. C. McIntyre, *Nature Materials*, 2011, **10**, 539.
17. N. C. Strandwitz, D. J. Comstock, R. L. Grimm, A. C. Nichols-Nielander, J. Elam and N. S. Lewis, *The Journal of Physical Chemistry C*, 2013, **117**, 4931-4936.

18. D. Bae, B. Seger, P. C. Vesborg, O. Hansen and I. Chorkendorff, *Chem Soc Rev*, 2017, **46**, 1933-1954.
19. B. Mei, A. A. Permyakova, R. Frydendal, D. Bae, T. Pedersen, P. Malacrida, O. Hansen, I. E. L. Stephens, P. C. K. Vesborg, B. Seger and I. Chorkendorff, *The Journal of Physical Chemistry Letters*, 2014, **5**, 3456-3461.
20. D. Bae, B. Mei, R. Frydendal, T. Pedersen, B. Seger, O. Hansen, P. C. K. Vesborg and I. Chorkendorff, *ChemElectroChem*, 2016, **3**, 1546-1552.
21. R. Liu, Z. Zheng, J. Spurgeon and X. Yang, *Energy & Environmental Science*, 2014, **7**, 2504-2517.
22. P. Nunez, M. H. Richter, B. D. Piercy, C. W. Roske, M. Cabán-Acevedo, M. D. Losego, S. J. Konezny, D. J. Fermin, S. Hu, B. S. Brunschwig and N. S. Lewis, *The Journal of Physical Chemistry C*, 2019, **123**, 20116-20129.
23. D. Bae, S. Shayestehaminzadeh, E. Thorsteinsson, T. Pedersen, O. Hansen, B. Seger, P. Vesborg, S. Olafsson and I. Chorkendorff, *Solar Energy Materials and Solar Cells*, 2016, **144**, 758-765.
24. R. L. Smith, B. Kloeck and S. D. Collins, *Journal of The Electrochemical Society*, 1988, **135**, 2001-2008.
25. E. D. Palik, J. W. Faust, H. F. Gray and R. F. Greene, *Journal of The Electrochemical Society*, 1982, **129**, 2051-2059.
26. K. Sun, Nicole L. Ritzert, J. John, H. Tan, W. G. Hale, J. Jiang, I. Moreno-Hernandez, K. M. Papadantonakis, T. P. Moffat, B. S. Brunschwig and N. S. Lewis, *Sustainable Energy & Fuels*, 2018, **2**, 983-998.
27. M. R. Shaner, S. Hu, K. Sun and N. S. Lewis, *Energy & Environmental Science*, 2015, **8**, 203-207.
28. X. Zhou, R. Liu, K. Sun, D. Friedrich, M. T. McDowell, F. Yang, S. T. Omelchenko, F. H. Saadi, A. C. Nielander, S. Yalamanchili, K. M. Papadantonakis, B. S. Brunschwig and N. S. Lewis, *Energy & Environmental Science*, 2015, **8**, 2644-2649.
29. K. Sun, M. T. McDowell, A. C. Nielander, S. Hu, M. R. Shaner, F. Yang, B. S. Brunschwig and N. S. Lewis, *The Journal of Physical Chemistry Letters*, 2015, **6**, 592-598.
30. K. Oh, C. Mériadec, B. Lassalle-Kaiser, V. Dorcet, B. Fabre, S. Ababou-Girard, L. Joanny, F. Gouttefangeas and G. Loget, *Energy & Environmental Science*, 2018, **11**, 2590-2599.
31. D. K. Lee and K.-S. Choi, *Nature Energy*, 2017, **3**, 53-60.
32. P. M. M. C. Bressers, J. J. Kelly, J. G. E. Gardeniers and M. Elwenspoek, *Journal of The Electrochemical Society*, 1996, **143**, 1744-1750.
33. P. M. M. C. Bressers, S. A. S. P. Pagano and J. J. Kelly, *Journal of Electroanalytical Chemistry*, 1995, **391**, 159-168.
34. R. Alfonsetti, L. Lozzi, M. Passacantando, P. Picozzi and S. Santucci, *Applied Surface Science*, 1993, **70-71**, 222-225.
35. Y. Chen, K. Sun, H. Audesirk, C. Xiang and N. S. Lewis, *Energy & Environmental Science*, 2015, **8**, 1736-1747.
36. J. Lin and W. G. Breck, *Canadian Journal of Chemistry*, 1965, **43**, 766-771.
37. X. H. Xia and J. J. Kelly, *Electrochimica Acta*, 2000, **45**, 4645-4653.
38. P. Allongue, V. Costa-Kieling and H. Gerischer, *Journal of The Electrochemical Society*, 1993, **140**, 1018.

39. H. Seidel, L. Csepregi, A. Heuberger and H. Baumgartel, *Journal of The Electrochemical Society*, 1990, **137**, 3612.
40. K. Sato, M. Shikida, Y. Matsushima, T. Yamashiro, K. Asami, Y. Iriye and M. Yamamoto, *Sensors and Actuators A: Physical*, 1998, **64**, 87-93.
41. W. A. Pliskin and H. S. Lehman, *Journal of The Electrochemical Society*, 1965, **112**, 1013-1019.
42. G. Xu, Z. Xu, Z. Shi, L. Pei, S. Yan, Z. Gu and Z. Zou, *ChemSusChem*, 2017, **10**, 2897-2903.
43. G. Loget, B. Fabre, S. Fryars, C. Mériadec and S. Ababou-Girard, *ACS Energy Letters*, 2017, **2**, 569-573.
44. S. A. Lee, T. H. Lee, C. Kim, M. G. Lee, M.-J. Choi, H. Park, S. Choi, J. Oh and H. W. Jang, *ACS Catalysis*, 2018, **8**, 7261-7269.
45. M. Chakrabarti and E. Roberts, *Journal of the Chemical Society of Pakistan*, 2008, **30**, 817-823.
46. S. Ašperger, *Transactions of the Faraday Society*, 1952, **48**, 617-624.
47. C. A. P. Arellano and S. S. Martínez, *Solar Energy Materials and Solar Cells*, 2010, **94**, 327-332.
48. S. Haussener, C. Xiang, J. M. Spurgeon, S. Ardo, N. S. Lewis and A. Z. Weber, *Energy & Environmental Science*, 2012, **5**, 9922-9935.
49. Y. Chen, S. Hu, C. Xiang and N. S. Lewis, *Energy & Environmental Science*, 2015, **8**, 876-886.
50. E. L. Warren, H. A. Atwater and N. S. Lewis, *The Journal of Physical Chemistry C*, 2013, **118**, 747-759.
51. J. M. Spurgeon, M. G. Walter, J. Zhou, P. A. Kohl and N. S. Lewis, *Energy & Environmental Science*, 2011, **4**, 1772-1780.
52. E. Verlage, S. Hu, R. Liu, R. J. R. Jones, K. Sun, C. Xiang, N. S. Lewis and H. A. Atwater, *Energy & Environmental Science*, 2015, **8**, 3166-3172.
53. M. Costa and C. B. Klein, *Critical Reviews in Toxicology*, 2006, **36**, 155-163.